

RESEARCH ARTICLE

Open Access



# Physicochemical characteristics and seasonal variations of PM<sub>2.5</sub> in urban, industrial, and suburban areas in South Korea

Kyuchool Hwang<sup>1</sup> , Jeongho Kim<sup>2</sup> , Jae Young Lee<sup>3</sup> , Jong-Sung Park<sup>4</sup> , Sechan Park<sup>1</sup> , Gahye Lee<sup>1</sup> , Chang Hyeok Kim<sup>4</sup> , Pilho Kim<sup>4</sup> , Su Hyun Shin<sup>4</sup> , Kwang Yul Lee<sup>4</sup> , Joon-Young An<sup>4</sup>, Jungmin Park<sup>4</sup> and Jong Bum Kim<sup>1\*</sup>

## Abstract

Among countries that are a part of the Organization for Economic Co-operation and Development, South Korea is the most exposed to PM<sub>2.5</sub>. Despite the country having implemented various strategies to limit PM<sub>2.5</sub> emissions, its concentrations are still high enough to pose serious environmental and health concerns. Herein, we monitored various physicochemical properties of PM<sub>2.5</sub> across different regions in South Korea from January 1 to December 31, 2021. Specifically, the study area consisted of the city center, industrial complexes, and suburban areas. Before analyzing dynamics of emissions specific to each site, the Clean Air Policy Support System data for the three areas were compared to elucidate their respective primary emission sources. The particle concentrations for the three areas were 21.8–26.44 µg/m<sup>3</sup>, with the highest concentrations being observed in March. All the three areas exhibited high ratios of NO<sub>3</sub><sup>-</sup> across all seasons. The particle number concentrations in the three sites were 1.3–1.5 × 10<sup>7</sup>, and the peak points of the concentrations were different in every site: city center (40 nm), industrial complexes (60 nm), and suburban areas (80 nm). We also conducted potential source contribution function and conditional bivariate probability function analyses. These analyses were conducted to determine the inflow direction of the pollution sources for high PM<sub>2.5</sub> episodes. For the episodes that occurred in spring and winter, there were no differences in the PM<sub>2.5</sub> concentrations between the three sites. Overall, the insights gained from this study offer a framework for developing air-quality management policies in South Korea, specifically in the context of PM<sub>2.5</sub> emissions.

**Keywords** PM<sub>2.5</sub> concentration, South Korea, Spatial variation, Potential source contribution function, Conditional bivariate probability function, Clean Air Policy Support System

## 1 Introduction

In 2019, approximately 4.14 million deaths worldwide were attributed to high PM<sub>2.5</sub> concentrations. Notably, long-term exposure to high PM<sub>2.5</sub> concentrations has been linked to a variety of cardiorespiratory diseases, such as lung cancer or heart diseases (Giannadaki et al., 2016; Shi et al., 2022). Numerous countries across the globe have been working toward reducing PM<sub>2.5</sub> concentrations in the atmosphere. Despite these attempts, PM<sub>2.5</sub> emissions continue to pose global environmental and health concerns (Cai et al., 2018; Hou et al., 2019; Lim et al., 2020). Beyond the scope of health-related issues,

\*Correspondence:

Jong Bum Kim

kjb0810@cni.re.kr

<sup>1</sup> Seohaean Research Institute, Chungnam Institute, Hongseong 32258, Republic of Korea

<sup>2</sup> Fine Particle lab co., Ltd, Incheon 21315, Republic of Korea

<sup>3</sup> Department of Environmental and Safety Engineering, Ajou University, Suwon 16499, Republic of Korea

<sup>4</sup> Climate & Air Quality Research Department, National Institute of Environmental Research, Incheon 22689, Republic of Korea

the  $PM_{2.5}$  driven deterioration of air can influence sunlight absorption and cloud formation, thereby influencing climate change and global warming (Kumar et al., 2017; Park et al., 2021). According to the 2018 report of the Organization for Economic Co-operation and Development (OECD), the Republic of Korea (Korea) recorded the highest share of population exposure to excessive  $PM_{2.5}$ , among all the OECD member countries (Choi et al., 2019). Korea has recognized this issue and has developed an ambient air quality standard specifically focusing on  $PM_{2.5}$  since 2015. As of 2023, the country has 614 telemetering air quality monitoring stations (AQMSs) to monitor the  $PM_{10}$ ,  $PM_{2.5}$ ,  $SO_2$ ,  $CO$ ,  $NO_2$ , and  $O_3$  concentrations (MOE 2023).

The chemical composition of  $PM_{2.5}$  has been linked to a variety of health-related issues (Park et al., 2020). Therefore, it is imperative to systematically record and collect physicochemical data pertaining to these particles. However, as AQMSs only provide a simple mass concentration of  $PM_{2.5}$ , the physicochemical data of pollutants in the context of health-related effects are limited (Jain et al., 2020). Therefore,  $PM_{2.5}$  management requires not only the management of particle mass concentrations but also the development of reduction technologies and policies that consider the physiochemical features of  $PM_{2.5}$ .

Korea has developed air-quality management plans to address pollution across different scales (e.g., metropolitan, central, southern, and southeastern regions) to effectively reduce  $PM_{2.5}$  emissions (Choi et al., 2022). Air quality management plans that consider emissions at a regional scale can be effective for managing the  $PM_{2.5}$  concentrations. This is because  $PM_{2.5}$  concentrations exhibit huge regional variations, pointing to the value of segmenting their management. For instance, in Chungcheongnam Province, in the Central Korea, 28 of the 58 Korean coal-fired power plants are located in this region (KEPCO 2023). In addition to the four cities that have coal-fired power plants (i.e., Dangjin, Seosan, Taean, and Boryeong), Hongseong, Yesan, and Buyeo have the largest livestock production facilities in the country. In some regions (e.g., Cheongyang, Geumsan, and Gyeryong), agriculture is the main industry, resulting in these regions exhibiting emission patterns different from those observed in aforementioned cities. Despite these regions having different drivers of  $PM_{2.5}$  emissions, region-specific solutions have not been developed for them; instead, identical solutions have been applied to these clearly different regions. Therefore, the development of region-specific solutions will increase the efficiency at which  $PM_{2.5}$  are reduced across Korea. Air quality research centers are used in every region to analyze various dynamics of air pollutants at a small scale. Notably, AQMSs provide information only about the mass concentration of each

pollutant, whereas air quality research centers provide detailed data of the various components of  $PM_{2.5}$ .

In this study, we used the extensive physicochemical  $PM_{2.5}$  data in addition to the meteorological data for three regions in 2021 to analyze regional dynamics of  $PM_{2.5}$  concentrations. These regions were selected because they are characterized by distinct emission characteristics, which are representative of many regions across the country.

Approximately half of the population in South Korea resides in these regions. Prior to the analysis of study-area-specific data, we analyzed the emission characteristics of the study site using national emission inventory. Figure 1 illustrates the air pollutant emissions in the Seoul Metropolitan Area (SMA), Ansan-si (Gyeonggi Province), and Seosan-si (South Chungcheong Province). Owing to diverse emission sources and component ratios, it is necessary to establish and implement effective policies that can improve the air quality; however, these policies should be rooted in a thorough consideration of regional conditions. Our study provides a foundation that will facilitate the development of effective air quality management policies for the abovementioned regions.

## 2 Materials and methods

### 2.1 Study areas

We conducted detailed analysis of  $PM_{2.5}$  concentrations in three regions in South Korea, whose locations and characteristics are shown in Fig. 2. The Seoul Atmospheric Environment Research (SAR) center, which was established in 2008, is located in Eunpyeong-gu, Seoul (37°36'37"N, 126°56'1"E). This center provided the  $PM_{2.5}$  concentration data for Seoul, which is the capital of the Republic of Korea. Furthermore, Seoul is a megacity consisting of approximately 9.5 million residents. The city is densely populated and has a high daily population flow; thus, traffic is the main source of air pollution in the region. The city also records high emissions from nonindustrial combustion in residential areas (Choi et al., 2022). Due to the high emissions that characterize Seoul, several control policies have been implemented in the region to reduce  $PM_{2.5}$  emissions (Bae et al., 2020; Kang et al., 2020; Park et al., 2020).

The Gyeonggi Atmospheric Environment Research (GAR) center is in Ansan, Gyeonggi Province (37°19'12"N, 126°49'42"E), which comprises approximately 650,000 residents. In GAR, there are four industrial complexes, including a national industrial complex (i.e., within 15 km from the monitoring station), and the Yellow Sea, which is west of this region. Geographically, when the westerlies are dominant, the pollutants emitted

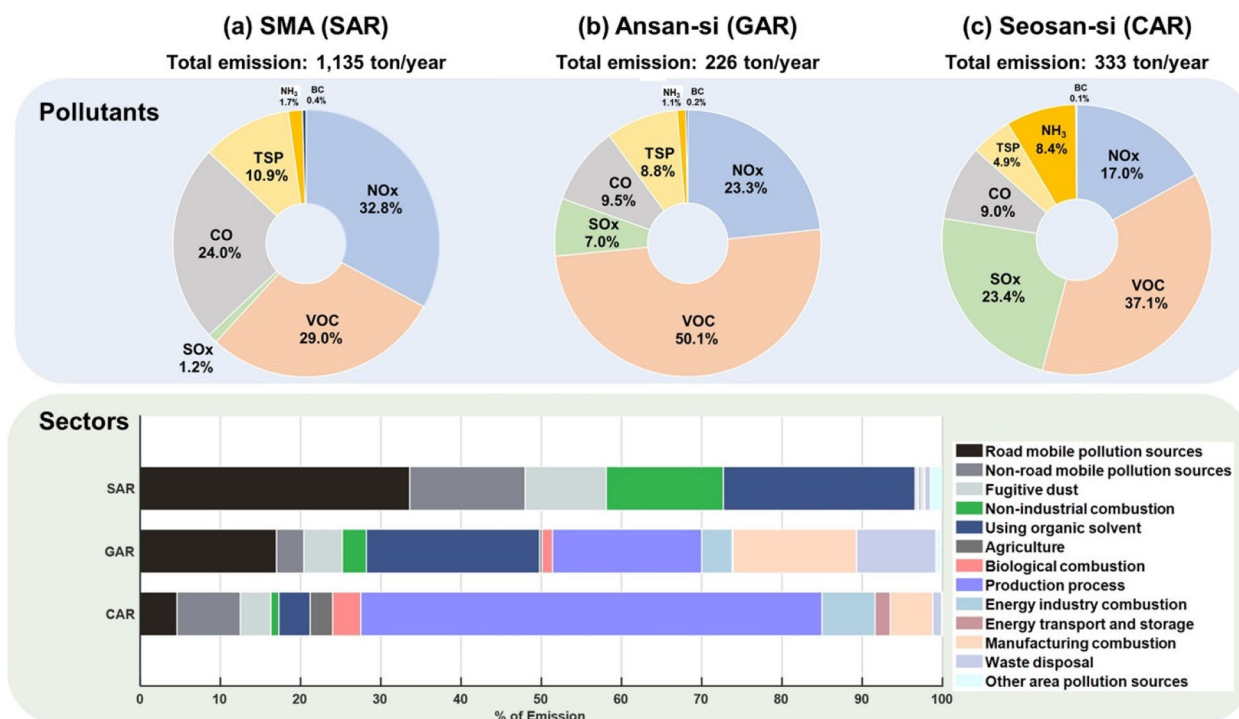


**Fig. 1** Contribution of different pollutants to emissions in each study area, along with the total emissions (upper panel) and the emission sources (lower panel). Seoul Atmospheric environment Research center (SAR), Gyeonggi Atmospheric environment Research center (GAR), Chungcheong Atmospheric environment Research center (CAR), total suspended particulate (TSP), volatile organic compounds (VOCs), black carbon (BC)

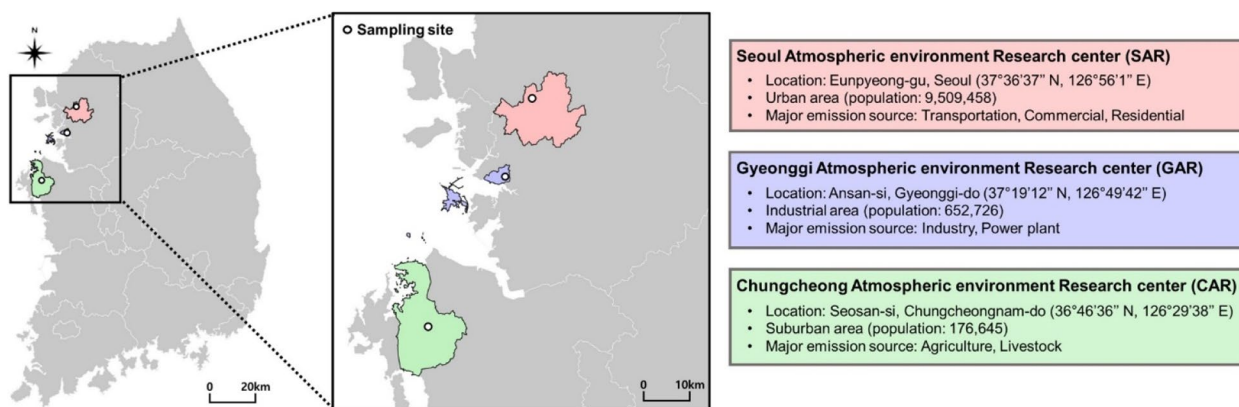


**Fig. 2** Locations of the study sites, along with the basic information and major emission sources for each area

from industrial complexes significantly impact the entire city.

The Chungcheong Atmospheric Environment Research (CAR) center is located in Seosan, Chungcheongnam Province (36°46'36"N, 126°29'38"E), which comprises approximately 180,000 residents. CAR is located at a distance of approximately 5 km from the city center, and there are farmlands and rural

areas around the monitoring site. In addition, there is a coal-fired power plant in Taean-gun, located to the west of CAR, and a petrochemical complex and a steelwork industry site are located north of the center. The presence of large-scale livestock production facilities and farmlands in the southeast region can result in considerable variations in regional emission characteristics, depending on the wind direction.

## 2.2 Measurements

We used the physicochemical data of  $PM_{2.5}$  representative of 1 year, specifically, from January 1, 2021, to December 31, 2021, to analyze the regional characteristics of the three stations. The measured variables included mass concentration, ions and metals contents, carbon components, and the particle number concentration of  $PM_{2.5}$ . In the context of meteorological data, we used data recorded by an automated synoptic observing system (ASOS) operated by the Korea Meteorological Administration at the station. Additionally, we used a  $\beta$ -ray absorption instrument (BAM 1020, Met One Instruments, Grants Pass, OR, USA) to analyze the mass concentration of  $PM_{2.5}$ . Briefly, the inlet of the measuring instrument was positioned at a height of approximately 40 m from the ground. In addition, including the roof level, the length of the pipe from the inlet to the measuring instrument was approximately 5 m. After sampling, the measurement tube was installed vertically to minimize the transfer loss of the sample; the stainless steel of the tube also minimized the transfer loss.

Furthermore, we analyzed the ion and metal components of  $PM_{2.5}$  using the gravimetric method. Briefly, samples collected continuously for 24 h through filters were analyzed using ion chromatography (AIM 9000D, URG Corporation, Chapel Hill, NC, USA) and X-ray fluorescence (XRF 625i, Cooper Environmental Services, Beaverton, OR, USA). Additionally, we analyzed eight ions (i.e.,  $NO_3^-$ ,  $SO_4^{2-}$ ,  $NH_4^+$ ,  $Cl^-$ ,  $Na^+$ ,  $Ca^{2+}$ ,  $Mg^{2+}$ , and  $K^+$ ) and 17 elements (Si, S, K, Ca, Ti, V, Cr, Mn, Fe, Ni, Cu, Zn, As, Se, Br, Ba, and Pb). And the thermal optical transmittance method (SOCEC model5, Sunset, OR, USA) was used to determine the concentration of carbonaceous compounds. Finally, to measure the particle number concentration, the scanning mobility particle sizer (model 3938L50, TSI Incorporated, Shoreview, MN, USA) was used; these measurements were conducted in the following range: 20–500 nm. Details of the equipment can be found in Park et al. (2013). Overall, the measured data was stored hourly in a data logger, and a total of 8659 data sets were constructed for all measurement sites.

## 2.3 Data analysis

### 2.3.1 Conditional bivariate probability function (CBPF)

We used the CBPF to track the direction and pathways of local  $PM_{2.5}$  pollution sources for every site. The CBPF, an extension of the conditional probability function (CPF), can be used to estimate the locations of high-concentration pollution sources in a region while accounting for wind direction and speed (Kim & Hopke, 2004; Uria-Tellaetxe & Carslaw, 2014). Notably, the CBPF model is

an extension of a 2-D probability model, which is based on a 3-D concept used to determine pollutant concentrations. We employed the “openair” package of R studio. This calculation was conducted using Eq. (1) as follows:

$$CBPF_{\Delta\theta, \Delta u} = \frac{m_{\Delta\theta, \Delta u} | y \geq C \geq x}{n_{\Delta\theta, \Delta u}} \quad (1)$$

where  $m_{\Delta\theta, \Delta u}$  is the number of data in the region with concentration  $C$  (between sections  $x$  and  $y$ ), when wind direction and speed are  $\Delta\theta$  and  $\Delta u$ , respectively, and  $n_{\Delta\theta, \Delta u}$  refers to the number of total data recorded for the entire area. In this study, we targeted the top 30% to analyze the effect of high  $PM_{2.5}$  concentration in each region.

### 2.3.2 Potential source contribution function (PSCF)

The CBPF allows for the elucidation of the direction of regional pollution sources; however, its effectiveness is limited to local scales. In Korea, air quality is affected not only by domestic emissions but also by long range transport of air pollutants from adjacent countries (Han et al., 2021; Seo et al., 2017). Therefore, we utilized PSCF modeling to determine the sources of the emissions that were transported into the three regions. Notably, PSCF modeling is generally used for estimating the potential pollution sources in a regional scale and simulating their air trajectories to the receptor points (Pekney et al., 2006; Zong et al., 2018); PSCF modeling requires the simulation of backward trajectory and meteorological field data. With regard to the backward trajectory data, we used values generated from the Hybrid Single-Particle Lagrangian Integrated Trajectory 4 (HYSPPLIT 4) model of the National Oceanic and Atmospheric Administration/Air Research Laboratory (NOAA/ARL). In terms of the meteorological field data, we used the Global Data Assimilation System 1 (GDAS 1) provided by the National Centers for Environmental Prediction (NCEP). The temporal and spatial resolutions of the model were set to 1 h and  $1^\circ$ , respectively, and the starting altitude was set to 500 m; this was done to reduce the effect of surface friction and to account for the wind in the lower boundary layer (Ara Begum et al., 2005). The backward trajectory simulation time was set to 48 h. The PSCF modeling was performed using Eq. (2):

$$PSCF_{ij} = \frac{m_{ij}}{n_{ij}} \quad (2)$$

where  $n$  refers to the number of total endpoints within a set grid ( $1^\circ \times 1^\circ$ ) and  $m$  refers to the number of endpoints of high-concentration trajectories above the threshold within a set grid. In general, when a PSCF model simulation had higher uncertainties, e.g., in the case of a grid having a relatively smaller number of endpoints, we



applied the weight function  $W(n_{i,j})$ . In this study, we applied the weight to a grid point lower than thrice the average endpoint number of the grid (Eq. 3) (Byun et al., 2022; Zhang et al., 2015; Zong et al., 2018).

$$W(n_{i,j}) = \begin{cases} 1.0 & 3N < n_{i,j} \\ 0.7 & N < n_{i,j} \leq 3N \\ 0.4 & N/2 < n_{i,j} \leq N \\ 0.2 & n_{i,j} \leq N/2 \end{cases} \quad (3)$$

where  $W(n_{i,j})$  refers to weight function and  $N$  refers to the number of total endpoints.

### 3 Results and discussion

#### 3.1 Meteorological data

We used ASOS data recorded by the Korea Meteorological Administration to analyze the meteorological data for every region throughout the study (Fig. 3). At the SAR, the main wind directions were northeasterly and westerly, with an average wind speed of 2.3 m/s; the frequency of calm winds was the lowest (for wind speed < 0.5 m/s) at 3.2%. The average temperature at this site was similar (13.7 °C) to that of the other regions, and the average humidity was the lowest (65.6%) among all the three sites. As the SAR is located inland (unlike GAR and CAR), it had lowest average humidity among all the three sites. At the GAR, the main wind directions were northwesterly and southeasterly, and frequency of calm winds was 14.1%, which was approximately four times than that of the SAR. As the average wind speed was the lowest (1.9 m/s) at the GAR, this could have been indicative of this region having the highest levels of pollution. At the CAR, diverse wind directions were prevalent in every season; the northeasterly wind was highly dominant, but the northwesterly wind was stronger (3 m/s). The frequency of calm winds was the highest (19.4%) at this

location compared to that in the other two sites; however, its regional impact was relatively weak owing to the frequent occurrences of strong winds in the coastal areas. The lowest temperature (i.e., in winter) recorded in this region was -19.3 °C, which was the lowest compared to the other two sites, and the average humidity was 73.4%. The wind rose diagrams for the three sites, for each season, are shown in Figure S1.

#### 3.2 Characteristics of particulate matter (PM<sub>2.5</sub>) mass concentrations and chemical composition at each study site

The annual average concentration of PM<sub>2.5</sub> (Fig. 4) at the SAR was 21.8 ± 17.7 µg/m<sup>3</sup>, while those at the GAR and CAR were 26.44 ± 22.70 µg/m<sup>3</sup> and 23.37 ± 22.29 µg/m<sup>3</sup>, respectively. The seasonal PM<sub>2.5</sub> concentrations at the SAR and GAR were the highest in spring (March–May) (24.88 ± 19.15 µg/m<sup>3</sup> and 32.14 ± 27.33 µg/m<sup>3</sup>, respectively), while those at the CAR were the highest in winter (November–January) (29.21 ± 18.88 µg/m<sup>3</sup>). The Korean government implemented the seasonal fine dust management system to reduce the emission of precursors from December to March of next year and eventually reduce the PM<sub>2.5</sub> emissions by controlling SO<sub>2</sub> and NO<sub>x</sub> emissions (Kang & Kim, 2022). However, high PM<sub>2.5</sub> were still observed because there are many coal-fired power plants in Chungcheongnam-do where CAR is located, which emit large quantities of air pollutants during winter. In contrast, for all the three sites, their lowest PM<sub>2.5</sub> concentrations were recorded in summer (June–August) (18.06 ± 12.21 µg/m<sup>3</sup>, 20.21 ± 13.46 µg/m<sup>3</sup>, and 14.97 ± 12.55 µg/m<sup>3</sup>, respectively). Specifically, concentrations of PM<sub>2.5</sub> at all the sites were the lowest in September; however, they increased in October, peaked in March, and finally decreased. In Northeast Asia, including the Republic of Korea, the emissions of

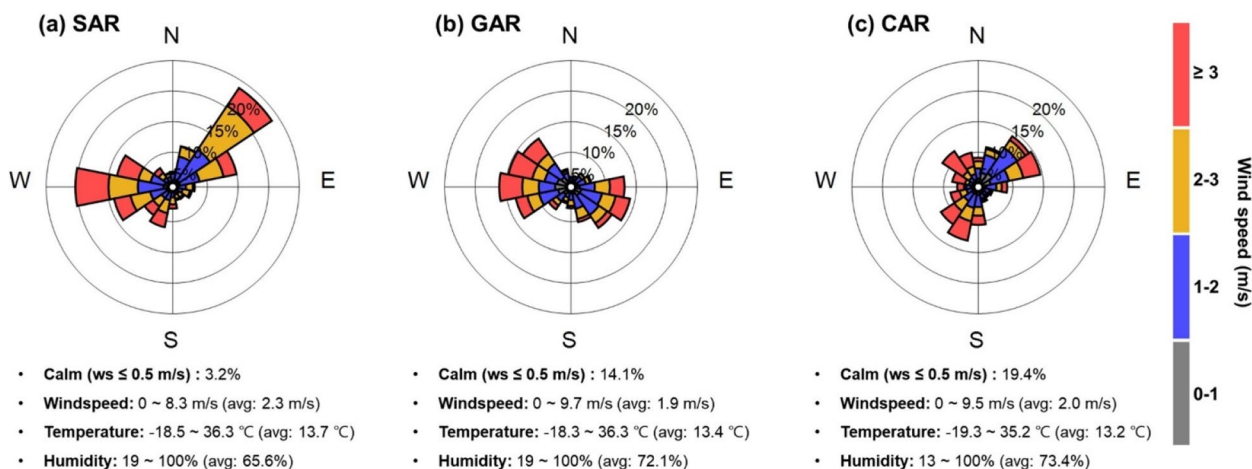


**Fig. 3** Wind rose diagrams and meteorological statistics at each site for 2021 based on the automated synoptic observing system (ASOS) data

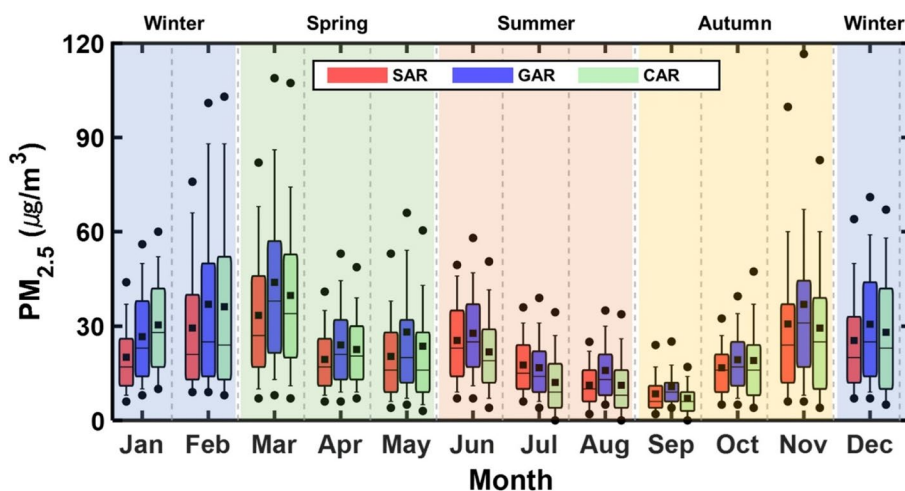


**Fig. 4** Monthly and seasonal variations in the PM<sub>2.5</sub> concentration at each site throughout 2021. Lower end and upper end of the box indicate the 25th and 75th percentiles, respectively; middle line and black square in the box indicate the median and average, respectively; lower and upper whiskers indicate the 10th and 90th percentiles, respectively; and black dots indicate the outliers

precursors and meteorological conditions change significantly depending on the season; overall, these changes result in distinct seasonal dynamics in the context of the concentration and composition of PM<sub>2.5</sub> (Bae et al., 2020; Shin et al., 2022).

The emissions of PM<sub>2.5</sub> precursors, including SO<sub>2</sub> and NO<sub>x</sub>, exhibit significant regional variation (Fig. 1) (Choi et al., 2021). According to the Korea-United States Air Quality (KORUS-AQ) field study conducted in 2016, the PM<sub>2.5</sub> concentrations in South Korea served an important role in the formation and growth of secondary particles (KORUS-AQ 2017; Bae et al., 2020). Figure 5 shows the percentage of PM<sub>2.5</sub> components in each site throughout the study. All three sites exhibited a tendency of having a high percentage of unknown components; this trend could be attributable to unmeasured organic components (Riva et al., 2015; Tao et al., 2014). These were unmeasured likely due to sampling losses or issues linked to the observation equipment. Previous studies have indicated that

unknown components may account for 20–35% of the total PM<sub>2.5</sub> percentage (Chen et al., 2019; Huang et al., 2014). As organic matter (OM) was not measured directly, as per previous studies, we calculated it by applying the conversion factor (1.6) to the value of organic carbon (OC) measured in this study (Liu et al., 2022; Turpin & Lim, 2001). Recently, various studies have begun to convert OC to OM; therefore, most of the conversion coefficients applied here use the values suggested in previous studies. Most of these conversion coefficients stem from studies that used high-tech equipment, such as HR-ToF-AMS; however, there are still not enough such studies worldwide. Therefore, we applied the same value to all points.

All the three sites had high proportions of NO<sub>3</sub><sup>-</sup> and OM, and SO<sub>4</sub><sup>2-</sup> and NH<sub>4</sub><sup>+</sup> were the second-highest components at all the sites. The CAR, which was classified as a suburban area in this study, exhibited a lower proportion of NO<sub>3</sub><sup>-</sup> than the two other sites and high proportions of OM and unknown components. Within the

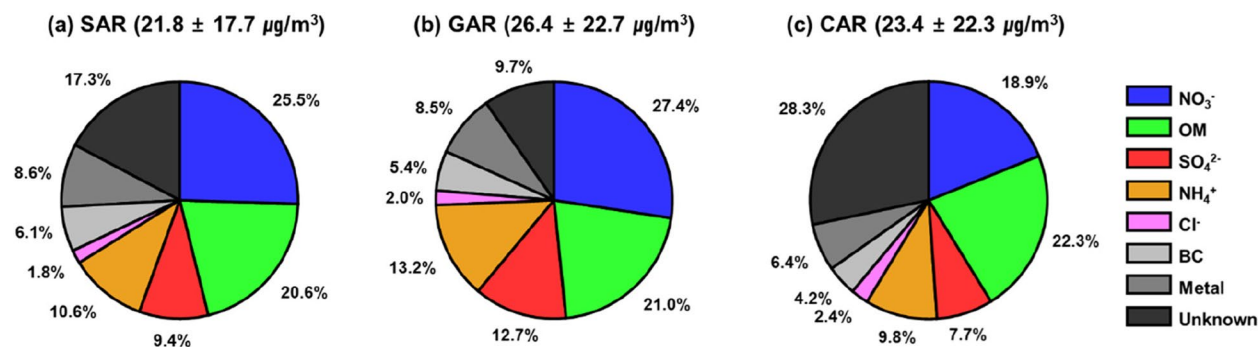


**Fig. 5** Average chemical composition of particulate matter (PM<sub>2.5</sub>) at each site in 2021

vicinity of the CAR, agricultural and livestock activities were predominant; therefore, the proportion of OC components was high due to the burning of biomass in this region, and the proportion of unknown components was high due to the influence of other unmeasured crustal materials and the marine particles from the ocean. Table S1 shows the average element concentrations observed throughout the monitoring period (see Table S1). CAR exhibits notably higher concentrations than regions in elements, such as Si, K, Cr, and Mn. Furthermore, the annual average chloride ion concentration was also 1.4–3.5 times higher than that of SAR and GAR. These trends are suggestive of the significant potential impact of marine aerosol and the crustal elements. The composition ratios of PM<sub>2.5</sub> were different in each region, depending on the seasonal changes (Fig. S2, Table S2). The proportion of SO<sub>4</sub><sup>2-</sup> increased in summer, while that of NO<sub>3</sub><sup>-</sup> increased in winter. These results are similar to those of previous studies that analyzed seasonal characteristics underlying PM<sub>2.5</sub> emissions. These results could be attributed to the increase in recorded air pollution due to meteorological conditions (e.g., high humidity in summer and high fuel consumption in winter) (Bell et al., 2007; Xie et al., 2019). An efficient PM<sub>2.5</sub> management policy will necessitate accounting for the control targets and main emission sources, based on the component ratio of seasonal chemical species.

Carbonaceous aerosols are generally classified into OC and elemental carbon (EC). OC is emitted by natural sources or secondary organic carbons through atmospheric oxidizers and photochemical reactions. In contrast, EC mainly occurs as a direct primary emission of fossil fuel combustion (Pio et al., 2011; Szidat et al., 2009). The OC/EC ratio can greatly differ, based on the fuel

type, quantity/amount of fuel, and combustion efficiency (Bhowmik et al., 2021). In this study, we analyzed the OC/EC ratio to specifically identify the regional and seasonal characteristics of PM<sub>2.5</sub> at each site (Fig. 6). During the entire observation period, the average values of the OC/EC ratios for the three sites were as follows: SAR (4.46), GAR (5.29), and CAR (5.98). From a seasonal perspective, the results were as follows: spring (4.29–5.55), summer (5.29–8.91), autumn (4.34–5.63), and winter (3.84–5.01), indicating that the values were high in summer and low in winter. Previous studies have indicated that the OC/EC ratios vary based on the pollution source types; the differences could be attributed to the type of combustion, e.g., automobile combustion (1.0–4.2), coal combustion (2.5–10.5), and biomass combustion (7.7). When the OC/EC ratio is above 2.0, secondary organic carbon (SOC) is actively generated by photochemical reactions (Schauer et al., 2002). The OC/EC ratio was the highest at the CAR site in summer (8.91), and the generation of SOC was the most active at this site as well. Alongside power plant emissions, CAR is near large agricultural and livestock operations. Consequently, there is a notably elevated proportion of OC during the summer in this region. The presence of these varied CAR emission sources implies that the OC–OM conversion factor for CAR could potentially exceed the value of 1.6 used in this study. At the SAR and GAR centers, which are in the large city center and industrial areas, respectively, we observed only minimal changes throughout the year, with the regional characteristics being dependent on the emission sources. The low coefficient of determination (R<sup>2</sup>) values of the OC and EC indicated that the pollution sources were different (Bhowmik et al., 2021). Across all the three sites, the R<sup>2</sup> values were the lowest in summer (0.58, 0.51, and 0.67,

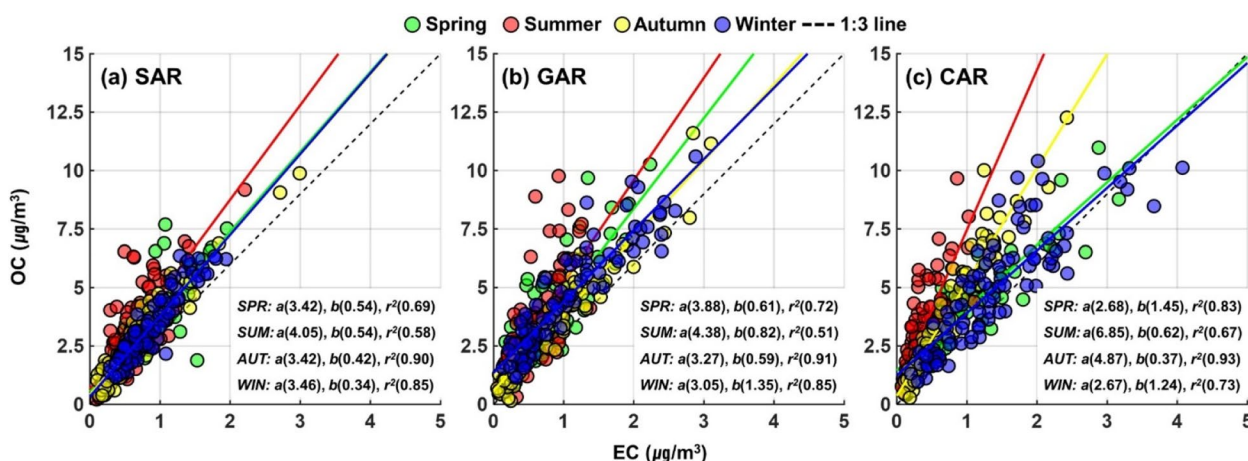


**Fig. 6** Scatter plots of OC/EC ratio during different seasons for each site. The slope (a), y-intercept (b), and r<sup>2</sup> of the regression line presented at the bottom right of each graph by season



respectively) and highest in autumn (0.90, 0.91, and 0.93, respectively). The  $R^2$  values were low due to the active generation of SOC, driven by the high temperature and oxidation of  $O_3$  in summer; in spring and winter, when the  $PM_{2.5}$  concentration was high, the  $R^2$  values were lower than the values observed in autumn due to the higher concentrations caused by the inflow of long-range trans-boundary pollutants.

### 3.3 Particle size distribution and particle formation characteristics

We considered a particle size distribution of 20–500 nm to analyze the particle number concentration characteristics of  $PM_{2.5}$  for every season (Fig. 7). The total particle number concentration range in spring was  $1.3\text{--}1.5 \times 10^7$ . No significant difference was found in the range itself, but the peak points were different for each site. The peaks of SAR, GAR, and CAR were 40, 60, and 80 nm, respectively. Geographically, when the sites were located in the southern regions, the size of the particles portrayed a pattern of growth. In summer, the peak points for the three sites were similar, but the total particle number concentrations portrayed the following order:  $GAR > SAR > CAR$ ; for the CAR site, we observed a decreasing trend in the particle size in summer. For the SAR and CAR, in autumn, we observed a decreasing trend in the particle size compared to the pattern observed in spring; however, at the GAR, there was an increase in the particle size. As indicated in Sect. 3.2, the average  $PM_{2.5}$  concentrations at the SAR and GAR were the highest in spring and lowest in summer, but there was no significant difference in the total

particle number concentration distribution. The higher concentration in spring could be attributed to higher concentrations of larger coarse particles, rather than assuming that the higher concentrations were driven by new particle formation (Park et al., 2015). The particle number concentration increased by approximately 30% in winter compared to that of other seasons. The average  $PM_{2.5}$  concentrations were the highest in spring and winter, but the particle number concentrations increased only in winter. Specifically, the high mass concentration observed during spring was likely attributable to the introduction of a limited number of coarse particles (e.g., yellow dust) from places beyond the study area. However, during winter, a high number of ultrafine particles (UFP) with sizes  $< 100$  nm were detected, which were attributed to combustion. This resulted in a concurrent increase in the number of particles and the weight concentrations of  $PM_{2.5}$ .

Figure 8 shows a scatter plot of the  $PM_{2.5}$ ,  $SO_4^{2-}$ , and  $NO_3^-$  concentrations for all the sites. Notably,  $NO_3^-$  and  $PM_{2.5}$  exhibited a high correlation at all three sites (0.85, 0.85, and 0.76 for SAR, GAR, and CAR, respectively), whereas  $SO_4^{2-}$  portrayed relatively low correlations (0.52, 0.55, and 0.44 for SAR, GAR, and CAR, respectively). At the sites, the slope of inorganic components and  $PM_{2.5}$  was 5.23–6.29 in  $SO_4^{2-}$ ; in the relatively low  $SO_4^{2-}$  concentration section ( $< 20 \mu\text{g}/\text{m}^3$ ), high-concentration  $PM_{2.5}$  ( $> 100 \mu\text{g}/\text{m}^3$ ) was generated.

In all three sites, the percentage of  $NO_3^-$  within  $PM_{2.5}$  was substantial. This observation is congruent with the emission dynamics shown in Fig. 1. SAR and GAR exhibit

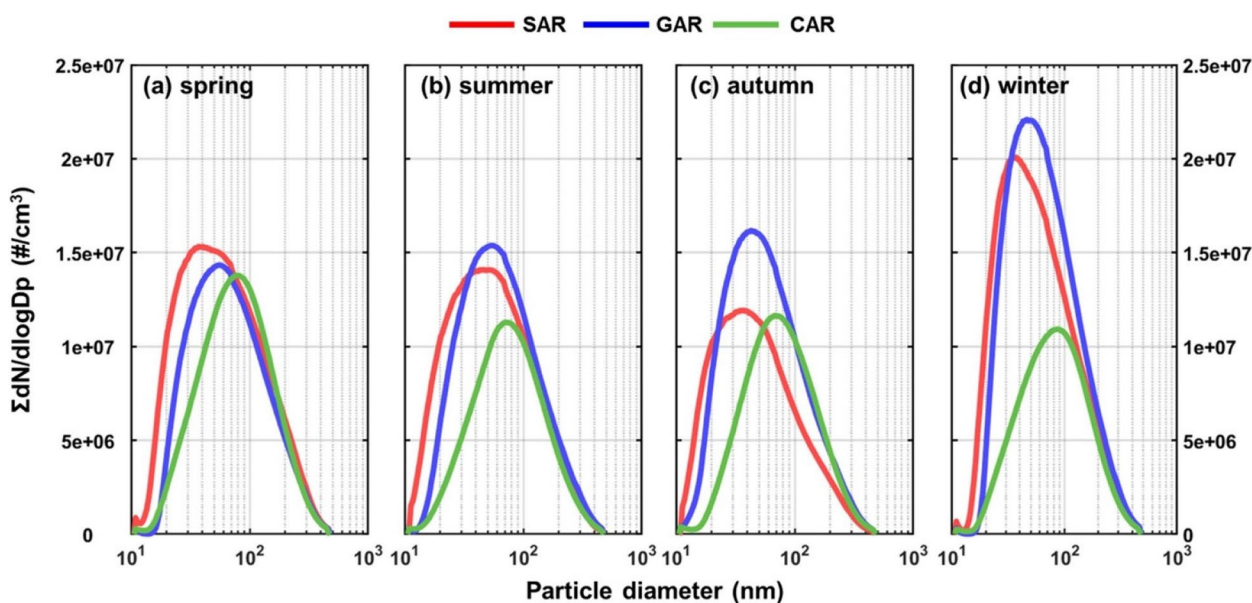
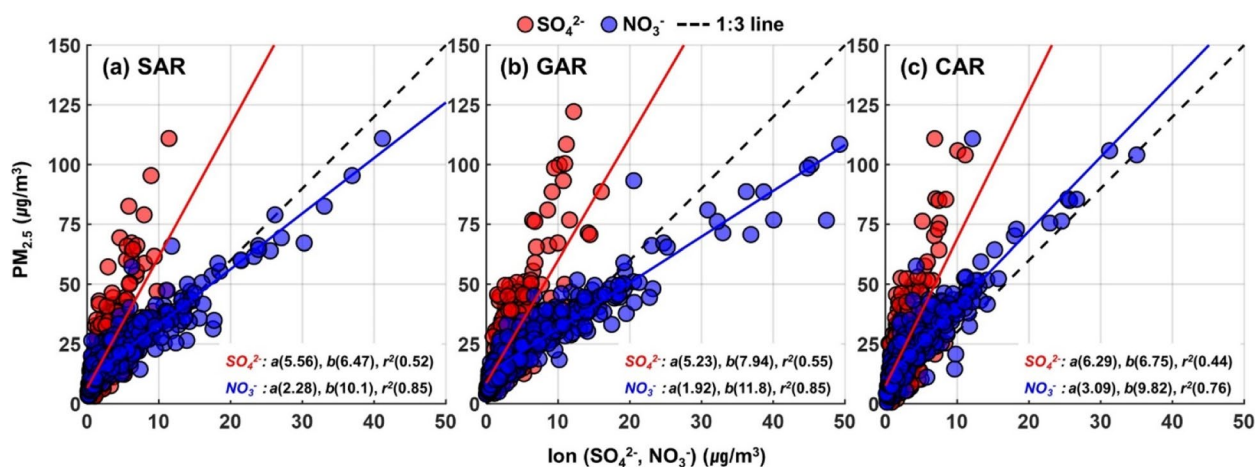


Fig. 7 Seasonal particle number size distribution at each site during 2021





**Fig. 8** Scatter plots of observed daily mean  $SO_4^{2-}$  and  $NO_3^-$  versus  $PM_{2.5}$  concentration at each site. Red and blue circles represent the concentration of  $SO_4^{2-}$  and  $NO_3^-$ , respectively. Slope, y-intercept, and  $r^2$  of the regression line are presented at the bottom right of each graph

a higher proportion of solvent utilization and road transportation than CAR, with  $NO_3^-$  playing a pivotal role in the formation of  $PM_{2.5}$ . Conversely, CAR demonstrates a relatively elevated  $PM_{2.5}$  fraction of organic matter and unknown compounds (see Fig. 5). Consequently, we infer that factors other than nitrate significantly contribute to the generation of  $PM_{2.5}$  in the CAR region.

In contrast to  $SO_4^{2-}$ ,  $NO_3^-$  displays exhibit a large amount of seasonal variation in its concentration, exhibiting a relatively modest correlation with  $PM_{2.5}$  (1.92–3.09 slope). As shown in Figure S2, during summer,  $SO_4^{2-}$  emissions occur, particularly when temperatures and relative humidity levels are high, and  $NO_3^-$  may undergo fragmentation and evaporation in high-temperature environments. In addition, other substances may also contribute to the generation of  $PM_{2.5}$  in summer (Bae et al., 2020). As suggested in previous studies, inorganic substances are crucial for controlling  $PM_{2.5}$  concentrations and reducing the concentrations of substances, such as  $NO_x$ ,  $SO_x$ , and VOCs (Bae et al., 2020). Given that the main precursors of secondary fine dust, i.e.,  $NO_x$  and VOCs, are directly involved in  $O_3$  generation, the concentration of  $O_3$  should be considered simultaneously as it is the strongest oxidizer in the atmosphere. Furthermore, the amount of emitted substances should be determined based on the results of atmospheric chemistry modeling to adjust the emission control substances and control amounts (Oak et al., 2019).

### 3.4 Analysis of high-concentration $PM_{2.5}$ episodes

For this study, we selected the high-concentration  $PM_{2.5}$  episodes that occurred during the observation period. These episodes were then used to perform PSCF and CBPF modeling (Figs. 9 and 10). We selected a total of

four sections, where the peaks commonly appeared at the three sites, and the average  $PM_{2.5}$  concentrations were  $>75 \mu g/m^3$ , as the high-concentration sections. Notably, in South Korea,  $75 \mu g/m^3$  is the current threshold for issuing a warning for fine dust. The four episodes considered in this study were as follows: Episode 1 (E1, February 12–14, 2021), Episode 2 (E2, March 11–12, 2021), Episode 3 (E3, March 26–29, 2021), and Episode 4 (E4, November 19–21, 2021) (Fig. S3).

In the PSCF model, during the E1 period, potential pollution sources were clearly observed in the cities located near the Yellow Sea in all sites; the sources appeared weak in Tsing-tao and several parts in Dalian, China. The average  $PM_{2.5}$  concentrations at the SAR, GAR, and CAR centers were 61.1, 95.4, and 98.5  $\mu g/m^3$ , respectively; the value was the highest at the CAR center, with the concentration being approximately thrice higher than the annual average concentration. During the observation period, in terms of the chemical composition of  $PM_{2.5}$ , the proportion of  $NO_3^-$  increased by approximately 1.5 times the annual average at all the three sites. The ratios of  $SO_4^{2-}$  and OC decreased significantly, which may be due to the high  $PM_{2.5}$  concentrations driven by high fossil fuel consumption in the industrial complexes and cities located close to the Yellow Sea (Wang et al., 2019). During E2, the three sites exhibited different patterns. Specifically, at the SAR center, the emission sources near the Seoul Metropolitan Area appeared strong, and the influences from the eastern region appeared weak, due to the occurrence of air stagnation phenomenon. During this period, the chemical composition appeared almost similar to that observed in E1, with the average concentration being 64.2  $\mu g/m^3$ . As for the GAR center,

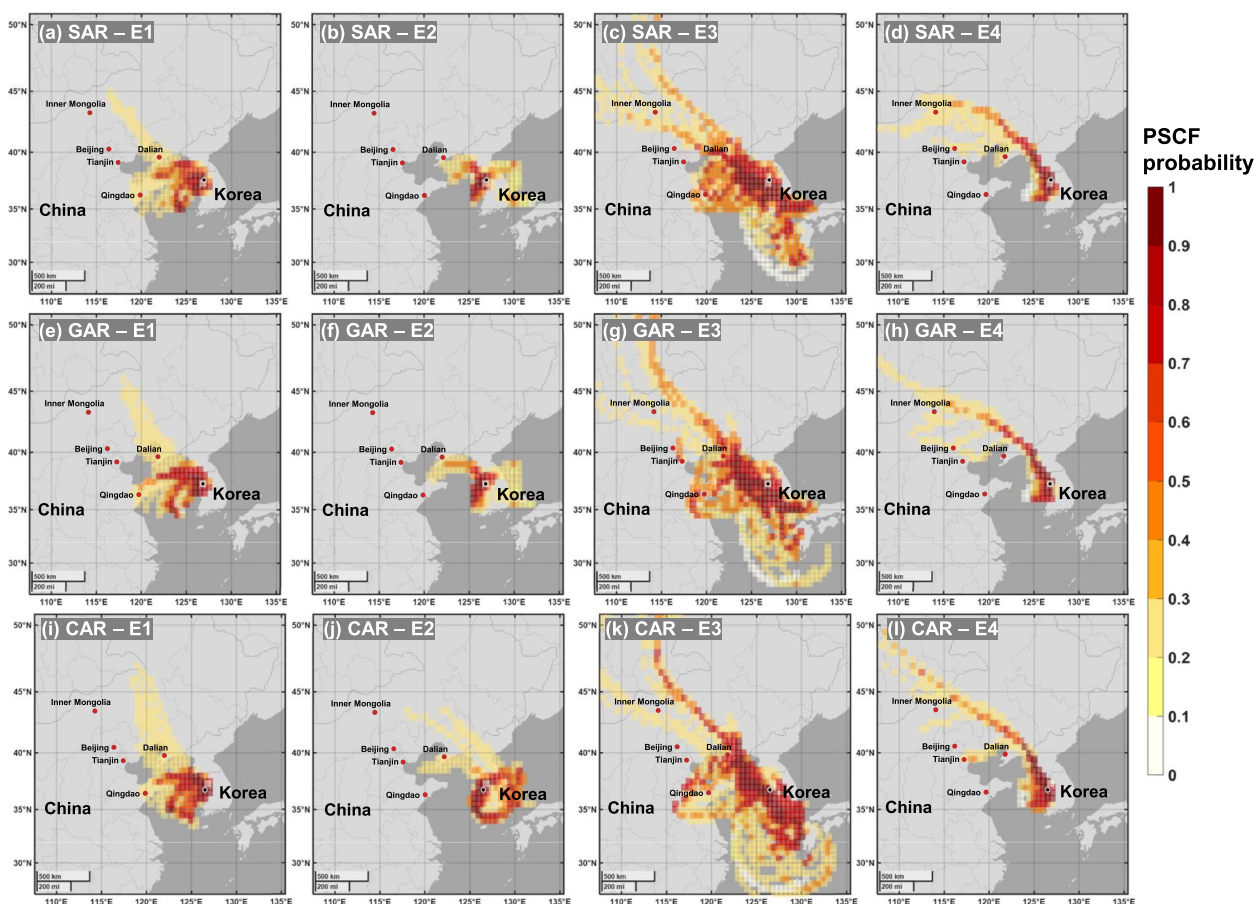


**Fig. 9** Potential source contribution function (PSCF) distribution results for particulate matter ( $PM_{2.5}$ ) concentrations at the three sites during Episode 1 (E1, February 12–14, 2021), Episode 2 (E2, March 11–12, 2021), Episode 3 (E3, March 26–29, 2021), and Episode 4 (E4, November 19–21, 2021). Red color represents the potential source areas. Black and red dots represent the receptor points and major cities in China, respectively

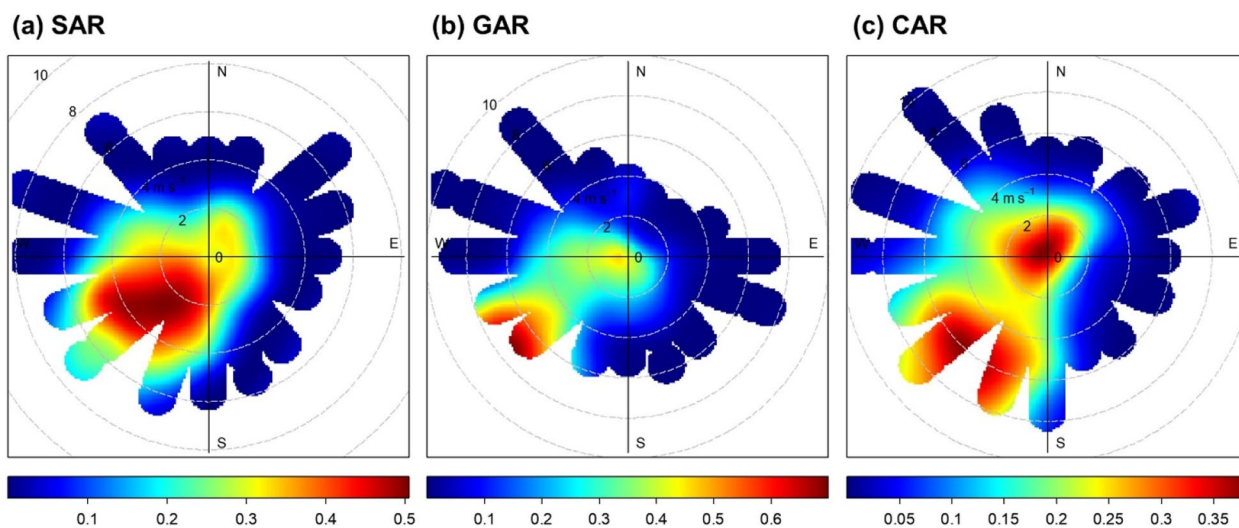


**Fig. 10** Conditional bivariate probability function (CBPF) results for particulate matter ( $PM_{2.5}$ ) concentrations at each site for 2021. Red color represents high potential source areas that affect pollutant concentrations

the Seoul Metropolitan Area and the areas around the Yellow Sea greatly influenced the chemical composition of  $PM_{2.5}$  concentration, as well as partial impacts from Darren. During E2, the average wind speed at the GAR site in spring was 2 m/s, and the ratio of constant temperature was 12.8% (Fig. S1). The areas around the Yellow Sea, which had potential pollution sources, and the substances emitted from Darren introduced high concentration of pollutants into the country with the westerlies, resulting in stagnation and, eventually, high-concentration cases. In terms of the CAR site, the pollutants could be introduced from several potential emission sources from the entire country and partially from Darren in China. During the E2 period, the ratio of  $NO_3^-$  decreased, whereas those of  $SO_4^{2-}$  and unknown components increased. There were no potential pollution sources in the inland areas in South Korea; however, we observed several along the coastal areas; this could be attributed to the high  $PM_{2.5}$  concentrations emitted from the industrial complexes, power plants, and ships near the coastal areas. During the E3 period, potential pollution sources were observed in all the three study sites. We observed potential sources throughout South Korea and the Darren and Qingdao regions in China, and some pollution sources were in the eastern areas of Mongolia. During this period, the ratios of metals and unknown components increased in all the three regions. In particular, in terms of the CAR site compared to E1, during E2, the content of metal and unknown components increased by approximately 2.5 and 1.5 times, respectively. Notably, the long-range transport of crustal elements in Mongolia contributed to higher crustal elements and metal components. During E3, we observed a mixed pattern of pollutants sourced from South Korea, Mongolia, and China, and the average  $PM_{2.5}$  concentrations during the period were the lowest among all episodes, at 43.2, 61.0, and 50.1  $\mu g/m^3$ , respectively. During E4, we observed similar patterns of potential pollution sources at all the three sites; therefore, we assumed that the main pollution sources originated from Inner Mongolia and the Shenyang region in China. Additionally, some potential pollution sources existed in parts of Tianjin and Beijing in China. During E4, the ratio of  $NO_3^-$  was the highest (35.3, 41.0, and 26.4% for SAR, GAR, and CAR, respectively), and the average concentrations were 91.5, 98.8, and 72.1  $\mu g/m^3$ , respectively, indicative of a slightly low concentration at the CAR center.

PSCF analysis can be conducted at scales greater than the regional scale, making this method suitable for global-scale studies, e.g., studies that entail simulating long-range transport and estimating the potential pollution sources. However, CBPF analysis may be more

effective for local-scale studies to analyze the direct impacts on corresponding points for a short time. In this study, we performed a CBPF analysis and compared the results with those obtained using PSCF (Figs. 10 and S5). Specifically, we used the top 30% concentration of the total average concentration as the analysis condition and analyzed the data for an entire year (Fig. 10) and all episode sections (Fig. S5) to eventually analyze the general characteristics of each site. For the SAR center, the high concentration of  $PM_{2.5}$  in 2021 was influenced by pollution sources in the southwest (Fig. 10a). Notably, 3 km to the southwest of the SAR site, there were large-scale residential and commercial complexes. Considering that the SAR site was a densely populated area, we could assume that pollutants associated with anthropogenic pollution affected the  $PM_{2.5}$  pollution sources at the corresponding point. Additionally, there were potential sources, such as the Gimpo International Airport, which was 13 km to the southwest of the site; these sources may have increased the  $PM_{2.5}$  concentrations in the region (Arunachalam et al., 2011). At the GAR site, the main pollution sources were located to the west and southwest (Fig. 10b). A large-scale industrial complex was located 5 km to the west of the GAR site, and the GAR site had a meteorological condition, in which the ratio of constant temperature was high throughout the year. Thus, the pollutants from the industrial complex were stagnant, culminating in high  $PM_{2.5}$  concentrations in the region.  $NO_x$  oxidation, which was the main emission from the industrial complexes, was converted into  $NO_3^-$ , resulting in a high ratio of  $NO_3^-$  during the high  $PM_{2.5}$ -concentration period (Fig. S4) (Wang et al., 2021). For CAR, the high-concentration  $PM_{2.5}$  pollution sources were located in the central and southwestern parts of the observation site (Fig. 10c); these regions had large-scale agricultural complexes, and there were thermal power plants 40 km to the south and 25 km to the northwest, as well as a petrochemical complex 25 km to the north of the site. As the CAR site was located at a distance from the main pollution sources, such as power plants, it did not experience direct impacts from the pollution sources, even when the wind flow was in the same direction. However, when the emitted substances reached CAR and the air was stagnant, there were significant impacts on the target sites. It is possible that  $PM_{2.5}$  could be generated by combining the ammonia emitted from several agricultural complexes, but additional studies will be necessary to support this idea. Thus, the PSCF and CBPF methods can be used for estimating the potential pollution sources in a region, but cautious interpretations are crucial when considering geographical-scale differences (Masiol et al., 2019).



## 4 Conclusions

Based on the data acquired from three air quality research centers representative of three regions in South Korea, we analyzed the physicochemical characteristics of PM<sub>2.5</sub> in each region and determined potential sources of pollution during high-concentration episodes. Notably, despite the abovementioned study sites being near each other, they brought forth different emission patterns. Regional pollutant management, which only focused on the Seoul Metropolitan Area in the past, is now being expanded to cover the entire country, which is a positive signal in the context of managing air quality. However, the current emission-oriented policies may be insufficient in the context of addressing issues linked to secondary emission sources and long-range transport. Therefore, the aim of this study was to provide insights that would facilitate improvements in the scale at which such measures can be implemented. Specifically, we analyzed various dynamics of PM<sub>2.5</sub> emissions at the three sites. Existing campaign-based studies have several disadvantages; it is difficult to obtain specific data, such as the annual changes in the areas, as the observations were conducted only in specific areas for particular periods. However, it seems possible to scrutinize the overall emission characteristics and distribution of PM<sub>2.5</sub> in each region if the data from all the air quality research centers in South Korea were used. Currently, there are 11 air quality research centers in South Korea, including the three centers considered in this study; the data from air quality research centers in each region can be fully utilized as the basic data for improving air quality policies while considering the regional emission characteristics. Overall, for this study, we only used the data representative of 1 year (2021) and considered only three regions. Future studies should utilize the annual data from more air quality research centers in other regions, elucidate regional characteristics and distribution of PM<sub>2.5</sub>, and design policies aimed at reducing PM<sub>2.5</sub> concentrations.

## Supplementary Information

The online version contains supplementary material available at <https://doi.org/10.1007/s44273-023-00018-5>.

**Additional file 1: Supplementary figures: Fig. S1.** Wind rose diagrams for each study site for 2021 for each season; Seoul Atmospheric environment Research center (SAR), Gyeonggi Atmospheric environment Research center (GAR), Chungcheong Atmospheric environment Research center (CAR). **Fig. S2.** Seasonal chemical composition of particulate matter (PM<sub>2.5</sub>) at each site in 2021; organic matter (OM), elemental carbon (EC), Seoul Atmospheric environment Research center (SAR), Gyeonggi Atmospheric environment Research center (GAR), Chungcheong Atmospheric environment Research center (CAR). **Fig. S3.** Time series of daily average PM<sub>2.5</sub> at each site and high-concentration episodes interval (yellow shading); Seoul Atmospheric environment Research center (SAR), Gyeonggi Atmospheric environment Research center (GAR), Chungcheong Atmospheric environment Research center (CAR); Episode 1 (E1, February

12–14, 2021); Episode 2 (E2, March 11–12, 2021); Episode 3 (E3, March 26–29, 2021); Episode 4 (E4, November 19–21, 2021). **Fig. S4.** Chemical composition of PM<sub>2.5</sub> at each site for Episode 1 (E1, February 12–14, 2021); Episode 2 (E2, March 11–12, 2021); Episode 3 (E3, March 26–29, 2021); Episode 4 (E4, November 19–21, 2021). **Fig. S5.** Conditional bivariate probability function (CBPF) results for PM<sub>2.5</sub> at each site during episode (E1–E4) period; E1, February 12–14, 2021); Episode 2 (E2, March 11–12, 2021); Episode 3 (E3, March 26–29, 2021); Episode 4 (E4, November 19–21, 2021). Red color represents high potential source areas affecting pollutants concentration; Seoul Atmospheric environment Research center (SAR), Gyeonggi Atmospheric environment Research center (GAR), Chungcheong Atmospheric environment Research center (CAR). Supplementary tables: **Table S1.** Annual mass concentration element components of PM<sub>2.5</sub> (unit: ng/m<sup>3</sup>). **Table S2.** Mass concentration of seasonal PM<sub>2.5</sub> and chemical components (unit: μg/m<sup>3</sup>).

## Authors' contributions

KH, conceptualization, data curation, formal analysis, resources, software, validation, visualization, writing—original draft, and review and editing. JK, conceptualization, resources, and investigation. JYL, conceptualization, investigation, and methodology. JSP, data curation, resources, and investigation. SP, software, validation, and investigation. GL, data curation, investigation, and visualization. CHK, data curation and investigation. PK, data curation and investigation. SHS, data curation and investigation. KYL, data curation, resources, and investigation. JYA, data curation, resources, and investigation. JP, conceptualization, resources, and investigation. JBK, conceptualization, supervision, and writing—review and editing.

## Funding

This research was conducted as part of a project entitled "The Study of source and evolution characteristics of submicron aerosols based on PM<sub>1.0</sub> and PM<sub>2.5</sub> analysis by NIER atmospheric research center (Grant number NIER-2023-04-02-056)" and funded by the Ministry of Environment (MOE) of the Republic of Korea. We would like to thank Editage ([www.editage.co.kr](http://www.editage.co.kr)) for English language editing.

## Availability of data and materials

Data will be made available on request.

## Declarations

### Competing interests

The authors declare that they have no competing interests.

Received: 1 July 2023 Accepted: 7 November 2023

Published online: 05 December 2023

## References

- Ara Begum, B., Kim, E., Jeong, C.-H., Lee, D.-W., & Hopke, P. K. (2005). Evaluation of the potential source contribution function using the 2002 Quebec forest fire episode. *Atmospheric Environment*, 39, 3719–3724. <https://doi.org/10.1016/j.atmosenv.2005.03.008>
- Arunachalam, S., Wang, B., Davis, N., Baek, B. H., & Levy, J. I. (2011). Effect of chemistry-transport model scale and resolution on population exposure to PM<sub>2.5</sub> from aircraft emissions during landing and takeoff. *Atmospheric Environment*, 45, 3294–3300. <https://doi.org/10.1016/j.atmosenv.2011.03.029>
- Bae, C., Kim, B.-U., Kim, H. C., Yoo, C., & Kim, S. (2020). Long-range transport influence on key chemical components of PM<sub>2.5</sub> in the Seoul metropolitan area, South Korea, during the years 2012–2016. *Atmosphere*, 11, 48. <https://doi.org/10.3390/atmos11010048>
- Bell, M. L., Dominici, F., Ebisu, K., Zeger, S. L., & Samet, J. M. (2007). Spatial and temporal variation in PM<sub>2.5</sub> chemical composition in the United States for health effects studies. *Environmental Health Perspectives*, 115, 989–995. <https://doi.org/10.1289/ehp.9621>



- Bhowmik, H. S., Naresh, S., Bhattu, D., Rastogi, N., Prévôt, A. S. H., & Tripathi, S. N. (2021). Temporal and spatial variability of carbonaceous species (EC; OC; WSOC and SOA) in PM<sub>2.5</sub> aerosol over five sites of Indo-Gangetic Plain. *Atmospheric Pollution Research*, 12, 375–390. <https://doi.org/10.1016/j.apr.2020.09.019>
- Byun, M., Park, J., Han, S., Kim, D. G., Jung, D.-H., & Choi, W. (2022). Spatial distributions of PM<sub>2.5</sub> concentrations, chemical constituents, and acidity for PM<sub>2.5</sub> pollution events and their potential source contribution: Based on observations from a nationwide air quality monitoring network for 2018–2019. *Journal of Korean Society for Atmospheric Environment*, 38, 508–523. <https://doi.org/10.5572/KOSAE.2022.38.4.508>. in Korean with English abstract
- Cai, S., Ma, Q., Wang, S., Zhao, B., Brauer, M., Cohen, A., Martin, R. V., Zhang, Q., Li, Q., Wang, Y., Hao, J., Frostad, J., Forouzanfar, M. H., & Burnett, R. T. (2018). Impact of air pollution control policies on future PM<sub>2.5</sub> concentrations and their source contributions in China. *Journal of Environmental Management*, 227, 124–133. <https://doi.org/10.1016/j.jenvman.2018.08.052>
- Chen, Y., Chen, Y., Xie, X., Ye, Z., Li, Q., Ge, X., & Chen, M. (2019). Chemical characteristics of PM<sub>2.5</sub> and water-soluble organic nitrogen in Yangzhou China. *Atmosphere*, 10, 178. <https://doi.org/10.3390/atmos10040178>
- Choi, J., Park, R. J., Lee, H.-M., Lee, S., Jo, D. S., Jeong, J. I., Henze, D. K., Woo, J.-H., Ban, S.-J., Lee, M.-D., Lim, C.-S., Park, M.-K., Shin, H. J., Cho, S., Peterson, D., & Song, C.-K. (2019). Impacts of local vs. trans-boundary emissions from different sectors on PM<sub>2.5</sub> exposure in South Korea during the KORUS-AQ campaign. *Atmospheric Environment*, 203, 196–205. <https://doi.org/10.1016/j.atmosenv.2019.02.008>
- Choi, S.-W., Bae, C., Kim, H.-C., Kim, T., Lee, H.-K., Song, S.-J., Jang, J.-P., Lee, K.-B., Choi, S.-A., Lee, H.-J., Park, Y., Park, S.-Y., Kim, Y.-M., & Yoo, C. (2021). Analysis of the National Air Pollutant Emissions Inventory (CAPSS 2017) data and assessment of emissions based on air quality modeling in the Republic of Korea. *Asian Journal of Atmospheric Environment*, 15, 114–141. <https://doi.org/10.5572/ajae.2021.064>
- Choi, S.-W., Cho, H., Hong, Y., Jo, H.-J., Park, M., Lee, H.-J., Choi, Y.-J., Shin, H.-H., Lee, D., Shin, E., Baek, W., Park, S.-K., Kim, E., Kim, H.-C., Song, S.-J., Park, Y., Kim, J., Baek, J., Kim, J., & Yoo, C. (2022). Analysis of the National Air Pollutant Emissions Inventory (CAPSS 2018) data and assessment of emissions based on air quality modeling in the Republic of Korea. *Asian Journal of Atmospheric Environment*, 16, 90–120. <https://doi.org/10.5572/ajae.2022.084>
- Giannadaki, D., Lelieveld, J., & Pozzer, A. (2016). Implementing the US air quality standard for PM<sub>2.5</sub> worldwide can prevent millions of premature deaths per year. *Environmental Health*, 15, 88. <https://doi.org/10.1186/s12940-016-0170-8>
- Han, X., Cai, J., Zhang, M., & Wang, X. (2021). Numerical simulation of interannual variation in transboundary contributions from Chinese emissions to PM<sub>2.5</sub> mass burden in South Korea. *Atmospheric Environment*, 256, 118440. <https://doi.org/10.1016/j.atmosenv.2021.118440>
- Hou, X., Chan, C. K., Dong, G. H., & Yim, S. H. L. (2019). Impacts of transboundary air pollution and local emissions on PM<sub>2.5</sub> pollution in the Pearl River Delta region of China and the public health, and the policy implications. *Environmental Research Letters*, 14, 034005. <https://doi.org/10.1088/1748-9326/aaf493>
- Huang, R.-J., Zhang, Y., Bozzetti, C., Ho, K.-F., Cao, J.-J., Han, Y., Daellenbach, K. R., Slowik, J. G., Platt, S. M., Canonaco, F., Zotter, P., Wolf, R., Pieber, S. M., Bruns, E. A., Crippa, M., Ciarelli, G., Piazzalunga, A., Schwikowski, M., Abbaszade, G., ... Prévôt, A. S. H. (2014). High secondary aerosol contribution to particulate pollution during haze events in China. *Nature*, 514, 218–222. <https://doi.org/10.1038/nature13774>
- Jain, S., Sharma, S. K., Vijayan, N., & Mandal, T. K. (2020). Seasonal characteristics of aerosols (PM<sub>2.5</sub> and PM<sub>10</sub>) and their source apportionment using PMF: A four year study over Delhi. *India. Environmental Pollution*, 262, 114337. <https://doi.org/10.1016/j.envpol.2020.114337>
- Kang, M., Kim, K., Choi, N., Kim, Y. P., & Lee, J. Y. (2020). Recent occurrence of PAHs and n-alkanes in PM<sub>2.5</sub> in Seoul, Korea and characteristics of their sources and toxicity. *International Journal of Environmental Research and Public Health*, 17, 1397. <https://doi.org/10.3390/ijerph17041397>
- Kang, Y.-H., & Kim, S. (2022). Seasonal PM Management: (1) What emissions should be reduced? *Journal of Korean Society for Atmospheric Environment*, 38, 746–763. <https://doi.org/10.5572/KOSAE.2022.38.5.746>. in Korean with English abstract
- Kim, E., & Hopke, P. K. (2004). Comparison between conditional probability function and nonparametric regression for fine particle source directions. *Atmospheric Environment*, 38, 4667–4673. <https://doi.org/10.1016/j.atmosenv.2004.05.035>
- Korea Electric Power Corporation (KEPCO). (2023). Coal fired power plant project status. <https://www.kepco-enc.com/eng/index.do>. Accessed 19 Mar. 2023
- Korea-United States Air Quality (KORUS-AQ). (2017). Introduction to the KORUS-AQ Rapid Synthesis Report. <https://espo.nasa.gov/sites/default/files/documents/KORUS-AQ-ENG.pdf>. Accessed 10 Feb. 2023
- Kumar, A., Singh, D., Anandam, K., Kumar, K., & Jain, V. K. (2017). Dynamic interaction of trace gases (VOCs, ozone, and NOx) in the rural atmosphere of sub-tropical India. *Air Quality, Atmosphere & Health*, 10, 885–896. <https://doi.org/10.1007/s11869-017-0478-8>
- Lim, C.-H., Ryu, J., Choi, Y., Jeon, S. W., & Lee, W.-K. (2020). Understanding global PM<sub>2.5</sub> concentrations and their drivers in recent decades (1998–2016). *Environment International*, 144, 106011. <https://doi.org/10.1016/j.envint.2020.106011>
- Liu, S., Geng, G., Xiao, Q., Zheng, Y., Liu, X., Cheng, J., & Zhang, Q. (2022). Tracking daily concentrations of PM<sub>2.5</sub> chemical composition in China since 2000. *Environmental Science & Technology*, 56, 16517–16527. <https://doi.org/10.1021/acs.est.2c06510>
- Masiol, M., Squizzato, S., Cheng, M.-D., Rich, D. Q., & Hopke, P. K. (2019). Differential probability functions for investigating long-term changes in local and regional air pollution sources. *Aerosol and Air Quality Research*, 19, Medium: ED; Size, 724–736. <https://doi.org/10.4209/aaqr.2018.09.0327>
- MOE (Ministry of Environment). (2023). Air quality monitoring station information. [https://www.airkorea.or.kr/eng/stationInformation?pMENU\\_NO=158](https://www.airkorea.or.kr/eng/stationInformation?pMENU_NO=158). Accessed 2 Feb. 2023
- Oak, Y. J., Park, R. J., Schroeder, J. R., Crawford, J. H., Blake, D. R., Weinheimer, A. J., Woo, J.-H., Kim, S.-W., Yeo, H., Fried, A., Wisthaler, A., & Brune, W. H. (2019). Evaluation of simulated O<sub>3</sub> production efficiency during the KORUS-AQ campaign: Implications for anthropogenic NO<sub>x</sub> emissions in Korea. *Elementa: Science of the Anthropocene*, 7. <https://doi.org/10.1525/elementa.394>
- Park, E. H., Heo, J., Kim, H., & Yi, S.-M. (2020). Long term trends of chemical constituents and source contributions of PM<sub>2.5</sub> in Seoul. *Chemosphere*, 251, 126371. <https://doi.org/10.1016/j.chemosphere.2020.126371>
- Park, M., Yum, S. S., & Kim, J. H. (2015). Characteristics of submicron aerosol number size distribution and new particle formation events measured in Seoul, Korea, during 2004–2012. *Asia-Pacific Journal of Atmospheric Sciences*, 51, 1–10. <https://doi.org/10.1007/s13143-014-0055-0>
- Park, S.-W., Choi, S.-Y., Byun, J.-Y., Kim, H., Kim, W.-J., Kim, P.-R., & Han, Y.-J. (2021). Different characteristics of PM<sub>2.5</sub> measured in downtown and suburban areas of a medium-sized city in South Korea. *Atmosphere*, 12, 832. <https://doi.org/10.3390/atmos12070832>
- Park, S.-S., Jung, S.-A., Gong, B.-J., Cho, S.-Y., & Lee, S.-J. (2013). Characteristics of PM<sub>2.5</sub> haze episodes revealed by highly time-resolved measurements at an air pollution monitoring supersite in Korea. *Aerosol and Air Quality Research*, 13, 957–976. <https://doi.org/10.4209/aaqr.2012.07.0184>
- Pekney, N. J., Davidson, C. I., Zhou, L., & Hopke, P. K. (2006). Application of PSCF and CPF to PMF-modeled sources of PM<sub>2.5</sub> in Pittsburgh. *Aerosol Science and Technology*, 40, 952–961. <https://doi.org/10.1080/02786820500543324>
- Pio, C., Cerqueira, M., Harrison, R. M., Nunes, T., Mirante, F., Alves, C., Oliveira, C., Sanchez de la Campa, A., Artíñano, B., & Matos, M. (2011). OC/EC ratio observations in Europe: Re-thinking the approach for apportionment between primary and secondary organic carbon. *Atmospheric Environment*, 45, 6121–6132. <https://doi.org/10.1016/j.atmosenv.2011.08.045>
- Riva, M., Tomaz, S., Cui, T., Lin, Y.-H., Perraudin, E., Gold, A., Stone, E. A., Villenave, E., & Surratt, J. D. (2015). Evidence for an unrecognized secondary anthropogenic source of organosulfates and sulfonates: Gas-phase oxidation of polycyclic aromatic hydrocarbons in the presence of sulfate aerosol. *Environmental Science & Technology*, 49, 6654–6664. <https://doi.org/10.1021/acs.est.5b00836>
- Schauer, J. J., Kleeman, M. J., Cass, G. R., & Simoneit, B. R. T. (2002). Measurement of emissions from air pollution sources. 5. C<sub>1</sub>–C<sub>32</sub> organic compounds from gasoline-powered motor vehicles. *Environmental Science & Technology*, 36, 1169–1180. <https://doi.org/10.1021/es0108077>
- Seo, J., Kim, J. Y., Youn, D., Lee, J. Y., Kim, H., Lim, Y. B., Kim, Y., & Jin, H. C. (2017). On the multiday haze in the Asian continental outflow: The important role of synoptic conditions combined with regional and local sources.

- Atmospheric Chemistry and Physics*, 17, 9311–9332. <https://doi.org/10.5194/acp-17-9311-2017>
- Shi, Y., Zhu, Y., Gong, S., Pan, J., Zang, S., Wang, W., Li, Z., Matsunaga, T., Yamaguchi, Y., & Bai, Y. (2022). PM<sub>2.5</sub>-related premature deaths and potential health benefits of controlled air quality in 34 provincial cities of China during 2001–2017. *Environmental Impact Assessment Review*, 97, 106883. <https://doi.org/10.1016/j.eiar.2022.106883>
- Shin, S. M., Lee, J. Y., Shin, H. J., & Kim, Y. P. (2022). Seasonal variation and source apportionment of oxygenated polycyclic aromatic hydrocarbons (OPAHs) and polycyclic aromatic hydrocarbons (PAHs) in PM<sub>2.5</sub> in Seoul, Korea. *Atmospheric Environment*, 272, 118937. <https://doi.org/10.1016/j.atmosenv.2022.118937>
- Szidat, S., Ruff, M., Perron, N., Wacker, L., Snyal, H. A., Hallquist, M., Shannigrahi, A. S., Yttri, K. E., Dye, C., & Simpson, D. (2009). Fossil and non-fossil sources of organic carbon (OC) and elemental carbon (EC) in Göteborg Sweden. *Atmospheric Chemistry and Physics*, 9, 1521–1535. <https://doi.org/10.5194/acp-9-1521-2009>
- Tao, S., Lu, X., Levac, N., Bateman, A. P., Nguyen, T. B., Bones, D. L., Nizkorodov, S. A., Laskin, J., Laskin, A., & Yang, X. (2014). Molecular characterization of organosulfates in organic aerosols from Shanghai and Los Angeles urban areas by nanospray-desorption electrospray ionization high-resolution mass spectrometry. *Environmental Science & Technology*, 48, 10993–11001. <https://doi.org/10.1021/es5024674>
- Turpin, B. J., & Lim, H.-J. (2001). Species contributions to PM<sub>2.5</sub> mass concentrations: Revisiting common assumptions for estimating organic mass. *Aerosol Science & Technology*, 35, 602–610. <https://doi.org/10.1080/02786820119445>
- Uria-Tellaetxe, I., & Carslaw, D. C. (2014). Conditional bivariate probability function for source identification. *Environmental Modelling & Software*, 59, 1–9. <https://doi.org/10.1016/j.envsoft.2014.05.002>
- Wang, H., Li, K., Li, J., Sun, Y., & Dong, F. (2021). Photochemical transformation pathways of nitrates from photocatalytic NO<sub>x</sub> oxidation: Implications for controlling secondary pollutants. *Environmental Science & Technology Letters*, 8, 873–877. <https://doi.org/10.1021/acs.estlett.1c00661>
- Wang, Y.-L., Song, W., Yang, W., Sun, X.-C., Tong, Y.-D., Wang, X.-M., Liu, C.-Q., Bai, Z.-P., & Liu, X.-Y. (2019). Influences of atmospheric pollution on the contributions of major oxidation pathways to PM<sub>2.5</sub> nitrate formation in Beijing. *Journal of Geophysical Research: Atmospheres*, 124, 4174–4185. <https://doi.org/10.1029/2019JD030284>
- Xie, Y., Liu, Z., Wen, T., Huang, X., Liu, J., Tang, G., Yang, Y., Li, X., Shen, R., Hu, B., & Wang, Y. (2019). Characteristics of chemical composition and seasonal variations of PM<sub>2.5</sub> in Shijiazhuang, China: Impact of primary emissions and secondary formation. *Science of the Total Environment*, 677, 215–229. <https://doi.org/10.1016/j.scitotenv.2019.04.300>
- Zhang, Z. Y., Wong, M. S., & Lee, K. H. (2015). Estimation of potential source regions of PM<sub>2.5</sub> in Beijing using backward trajectories. *Atmospheric Pollution Research*, 6, 173–177. <https://doi.org/10.5094/APR.2015.020>
- Zong, Z., Wang, X., Tian, C., Chen, Y., Fu, S., Qu, L., Ji, L., Li, J., & Zhang, G. (2018). PMF and PSCF based source apportionment of PM<sub>2.5</sub> at a regional background site in North China. *Atmospheric Research*, 203, 207–215. <https://doi.org/10.1016/j.atmosres.2017.12.013>

## Publisher's Note

Springer Nature remains neutral with regard to jurisdictional claims in published maps and institutional affiliations.